Journal of Intelligent & Robotic Systems (2024) 110:12
https://doi.org/10.1007/s10846-023-02047-2

REGULAR PAPER

CPG-Fuzzy Heading Control for a Hexapod Robot with Arc-Shaped Blade Legs

Yani Zhang[1] · Rongxin Cui[1] · Haoquan Li[1] · Xinxin Guo[1]

Received: 9 August 2023 / Accepted: 29 December 2023 / Published online: 16 January 2024

Abstract
Based on the central pattern generator (CPG) and fuzzy controller, this paper proposes a heading control method for the directional motion for a new type of blade legged hexapod robot (BLHR). First, the modified Hopf oscillator is used to construct the CPG model of BLHR based on the limit cycle. Second, the fuzzy controller is applied to adjust the support angles of legs to change the heading of BLHR, thereby correcting the error between the actual and desired heading angle in real-time. Finally, the feasibility and effectiveness of the proposed CPG-Fuzzy control method is verified in Gazebo simulations and real-world experiments. This is the first attempt to combine CPG and fuzzy control in the context of hexapod robot. In comparison to existing control methods, the proposed CPG-Fuzzy controller can implement heading control of BLHR with better performance and value of further investigation.

Keywords Central pattern generator · Hopf oscillator · Fuzzy control · Hexapod robot · Blade leg · Heading control

1 Introduction

In the realm of robotics research, legged robots hold great significance. These robots exhibit a high degree of limb articulation, affording them adaptability in their gait. They meticulously fine-tune the joint angles in their legs to maintain stable locomotion, making them particularly well-suited for operation in unstructured environments, as noted in [1]. Legged robots, on the other hand, generally suffer from relatively slower walking speeds and are susceptible to tipping due to shifts in their center of gravity. Conversely, wheeled robots offer rapid mobility, heightened efficiency, and simplified control mechanisms. However, their movement is largely confined to level surfaces, rendering them ill-suited for negotiating rugged terrains such as gullies and staircases. In response to these distinctions, researchers have ingeniously crafted wheel-legged mobile robots, amalgamating the merits of both legged and wheeled locomotion [2–5].

Wheel-legged mobile robots have attracted wide attention because of their advantages of high mobile speed and strong obstacle avoidance ability [6]. The hexapod robot RHex consisted of six semi-circular flexible legs, which can realize various typical motion modes such as running, jumping and climbing stairs, etc [7]. Whegs was a robot with six three-spoke wheel legs, each spoke alternating supported on the ground periodically. It has shown strong obstacle crossing ability and terrain adaptation [8]. The hybrid underwater hexapod robot HUHR had six C-shaped legs that combined the mobility of wheeled legs and the climbing ability of crab legs. Each leg had only one degree of freedom, making it easy to control. HUHR can achieve various motion modes such as cruising, walking and climbing [9]. The amphibious robot AmphiHex-II combined the advantages of curved legs on land with webbed legs underwater, and was capable of stable operation in water and on land [10].

Currently, the technology to study the structural design of mobile robots is much mature, but there are still many problems on gait planning and control [11]. As a key research field for the motion control of legged robots, appropriate gait planning not only ensures the stable adjustment of the robot in rugged environments, but also improves the energy

✉ Rongxin Cui
r.cui@nwpu.edu.cn

Yani Zhang
zhangyani@mail.nwpu.edu.cn

Haoquan Li
hqli@mail.nwpu.edu.cn

Xinxin Guo
guoxx@nwpu.edu.cn

[1] School of Marine Science and Technology, Northwestern Polytechnical University, 710072 Xi'an, China

efficiency and walking speed of the robots [12]. There are two main methods on gait planning for legged robots, i.e., model-based method and bionic method. Traditional model-based method relies too much on accurate robot model. Its kinematic calculations are notably complex, and trajectory planning poses a considerable challenge. Moreover, the associated workload is substantial, which hampers the feasibility of real-time control for legged robots. The bionics method is to plan the gait based on the external environment and stimuli by simulating the behavior of the biologically control leg movements [13]. It combines biological science and engineering techniques to achieve better adaptation and speed of response compared with traditional control methods. Central pattern generator (CPG) is one of the research hotspots in the field of bionic control. It simulates the self-excitation behavior of biological lower neural centers to produce rhythmic motion, which has been verified to be suitable for the motion control of multi-legged robots [14].

There are several kinds of oscillators widely used as CPG neurons, such as Matsuoka oscillator, Kimura oscillator, cosine oscillator, Van Del Pol oscillator and Hopf oscillator [15–19]. The main advantage of the Hopf oscillator, as compared to other oscillators, is the clear physical interpretation of its parameters. Moreover, it allows for independent adjustments of both amplitude and phase, rendering it a better option for generating gaits in hexapod robots. The modified Hopf oscillator was first proposed to realize the walking and trotting gait of the quadruped robot based on CPG control mode in [20]. The CPG control method and the modified Hopf oscillator was adopted in [21] to generate different gait of the quadruped robot. Altering the driving signal has the potential to induce variations in motion and velocity, facilitating smooth transitions between different gaits.

Regarding motion control, Lindqvist et al. [22] introduced a depth point heading regulation method employing depth images captured by airborne RGB-D cameras. They applied this heading regulation technique to govern the heading angle of quadruped robots. Additionally, a sliding mode tracking control scheme for a four wheel-legged robot was proposed [23] based on neural networks under uncertain interactions. This method guarantees minimal lateral and heading errors in the robot's tracking process. Controllers that only use CPG method belong to open-loop control, making it difficult to achieve real-time control of robots. Many scholars have combined CPG with other approaches. Yu et al. [24] proposed a method for determining optimized control parameters for multi-joint biomimetic robotic fish. The system performance was improved by combining the dynamic model and particle swarm optimization algorithm to find the characteristic parameters of CPG. A closed-loop sensory feedback control structure based on CPG for a biomimetic robotic fish was proposed in [25]. The closed-loop fuzzy logic control structure was used as a brain model to determine adaptive swimming modes based on sensory information. Yan et al. [26] proposed a model predictive controller based on CPG to achieve trajectory tracking control of the biomimetic robotic fish. A motion controller for undulating fin robot was proposed in [27]. The controller was composed of an modified CPG network, and the convergence rate was optimized by using reinforcement learning algorithm.

Inspired by the above analyses, we propose a CPG-Fuzzy controller to study the heading control of the blade legged hexapod robot (BLHR). The BLHR amalgamates the strengths of both legged and wheeled robots while exhibiting robust adaptability to varying terrains. The mapping function between CPG output and joint rotation angle can be changed by adjusting the support angle of the legs using the fuzzy controller. In this way, the real-time heading control is achieved. Gazebo simulations and real-world experiments are conducted to investigate and validate the performance of the proposed method.

Our main contributions are summarized as follows.

1. Diverging from the sole application of CPG control in hexapod robots as seen in previous studies [11, 18], we employ a CPG-Fuzzy controller for the heading control of hexapod robot that is driven by arc-shaped blade legs. This is due to the fact that both CPG and fuzzy control operate independently of accurate mathematical models, making them straightforward to compute and implement. To our knowledge, this is the first attempt to combine CPG and fuzzy control in the context of hexapod robots. By formulating fuzzy control rules rooted in practical experience, the control performance demonstrated in this paper is better than that of [9].
2. In this paper, we introduce an annular coupling network CPG structure for the BLHR. This structure exhibits greater coupling strength when contrasted with the chain structure, as seen in prior works [10, 27]. In comparison to fully connected network configurations [11], the annular coupling network reduces computational complexity while upholding control performance.
3. We conduct thorough simulations within the Gazebo environment and real-world experiments in an indoor hallway to showcase the practicality and efficacy of our proposed approach.

The remainder of this paper is organized as follows. Section 2 introduces the structure of BLHR and Hopf oscillator. The proposed CPG-fuzzy controller is designed in Section 3. Section 4 shows the simulation and experimental results. Finally, Section 5 concludes the work and gives the future direction.

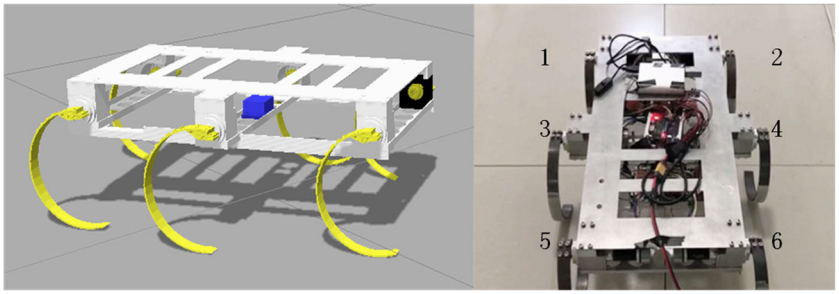

Fig. 1 Blade legged hexapod robot and its leg number

2 Preliminaries

2.1 The Structure of BLHR

The BLHR exhibits a symmetric structure, featuring a sleek and slender body. Its locomotion is driven by six identically sized arc-shaped blade legs, evenly distributed on either side of the body. The structural configuration of BLHR is presented in Fig. 1, with legs numbered from 1 to 6. Each leg possesses a single degree of freedom, actuated by an electric motor. The main structural parameters are detailed in Table 1.

The blade legs rotate full circle with counterclockwise, just as Fig. 2 shows. The state in which the blade leg is elevated above the ground is termed the swing phase, while the state where it makes contact with the ground is known as the support phase. Point P signifies the location where the blade leg transitions from the swing phase to the support phase, while point Q marks the position where this transition occurs from the support phase back to the swing phase. The angles at these critical points are denoted as θ_P for the blade leg at point P and θ_Q for the blade leg at point Q.

In a rotation cycle, the support angle is defined as $\theta_s = \theta_Q - \theta_P$, and the swing angle is defined as $\theta_f = 2\pi - \theta_s$. The height of leg joint from the ground can be expressed as

$$\begin{cases} h_P = R\cos(\pi - \theta_P) + R \\ h_Q = 2R\cos(\theta_Q - \pi). \end{cases} \tag{1}$$

From the geometric relationship in Fig. 2, it is clear that $h_P = h_Q$, then we can get the relationship between θ_P and θ_Q as

$$\theta_P = \arccos(1 + 2\cos\theta_Q). \tag{2}$$

Table 1 The main structure parameters of BLHR

Parameters	Description	Value(mm)
L	Length	580
W	Width	414
H	Height	210
R	Radius of blade legs	88

Remark 1 In mechanical design, in order to ensure the stability of the robot, the blade legs are required to have a certain stiffness, while the necessary elasticity is required to reduce the impact on the ground and achieve the shock absorption effect. Therefore, 65 Mn spring steel is selected as the material for the blade legs, and the maximum static load on a single leg is 4 Kg when the weight of the robot body is 8 Kg.

2.2 Hopf Oscillator

Based on the advantages of the Hopf oscillator analyzed earlier, in this paper, we select Hopf oscillator as the basic model of CPG, the mathematical model of a typical Hopf oscillator is expressed as follows

$$\begin{cases} \dot{x} = \alpha(\mu - x^2 - y^2)x - \omega y \\ \dot{y} = \alpha(\mu - x^2 - y^2)y + \omega x, \end{cases} \tag{3}$$

where x, y are the coupling variable, α is the convergence rate of the limit cycle, $\sqrt{\mu}$ is the steady-state amplitude of the oscillator and ω is the oscillator frequency.

The Hopf oscillator can produce sinusoidal waveform stably, with its output signal being dimensionless. The ascending part and descending part of y correspond to swing phase and support phase in the walking gait of the robot, respectively. Its duty cycle $\beta = 0.5$ generally, which means

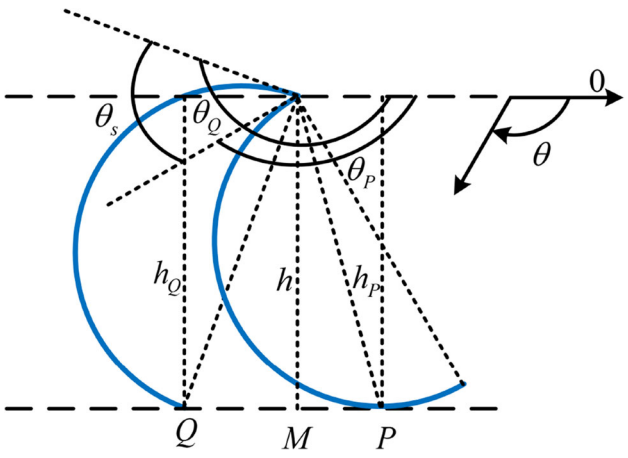

Fig. 2 Single leg rotation diagram

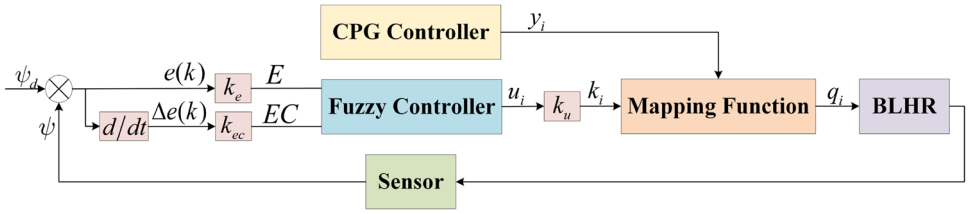

Fig. 3 The CPG-Fuzzy controller structure block diagram

the time of swing phase T_f equals to the time of support phase T_s. Define the gait cycle as $T = T_f + T_s$, then the relationships between time and β are $T_s = \beta T$ and $T_f = (1-\beta)T$. In the actual walking process, T_f and T_s are not necessarily the same, and different β makes the walking gait of hexapod robot diversely. In order to adjust the phase position between swing phase and support phase, an modified Hopf oscillator was proposed as the signal generator of hexapod robot [20]. Compared with typical Hopf oscillator, the modified oscillator frequency is designed as

$$\omega = \frac{\omega_f}{e^{-bx}+1} + \frac{\omega_s}{e^{bx}+1}, \tag{4}$$

where ω_f is the frequency of swing phase and ω_s is the frequency of support phase. b is the conversion speed between swing phase and support phase.

The swing phase and support phase can be adjusted independently by changing the ratio between ω_f and ω_s, i.e., $\omega_f : \omega_s = \beta : (1-\beta)$. In this way, output waveforms corresponding to different gaits are implemented.

3 CPG-Fuzzy Controller Design

In this section, we propose a CPG-Fuzzy controller to implement the heading motion of BLHR. The structure block diagram of the CPG-Fuzzy controller is illustrated in Fig. 3. Initially, the CPG model for BLHR is built using the modified Hopf oscillator. Subsequently, the fuzzy controller comes into play to generate the adjustment coefficient for the leg support angles. Finally, the joint rotation angles for all six legs are derived through a mapping function, facilitating real-time correction of any disparity between the actual and desired heading angles.

Remark 2 The primary emphasis of this paper centers on accomplishing both gait planning and heading control for the hexapod robot driven by arc-shaped blade legs. While gait planning can be realized through the biological CPG approach. There are various methods available for heading control. Much like CPG, fuzzy control operates without a strict dependence on the robot's mathematical model. Hence, we have chosen to integrate the CPG with the fuzzy controller as our approach.

3.1 Overall Structure of CPG Network

The biological CPG can be categorized into two primary structures: chain and network. In the chain CPG, oscillators are organized sequentially, maintaining a constant phase difference between each oscillator. The network CPG consists of multiple oscillators to form a network topology. Among these topologies, the annular and fully connected coupling network, depicted in Fig. 4, stands out as the most prevalent. It's evident that the annular coupling network's coupling strength resides in the middle of the three options. This configuration not only fulfills the communication requirements of the hexapod robot but also strikes a balance in terms of computational complexity.

The single leg of BLHR interact with each other and coordinate to complete the motion process. According to the structure characteristics and gait motion mode of BLHR, we construct the CPG network topology of the system as shown in Fig. 5. The network of whole system is composed of six oscillators which are coupled with each other according to the annular topological structure.

The mathematical model of annular coupled network can be expressed as

$$\begin{cases} \dot{X} = \alpha A X - W Y \\ \dot{Y} = \alpha A Y + W X + \varepsilon(\mathcal{M} Y - \mathcal{N} X), \end{cases} \tag{5}$$

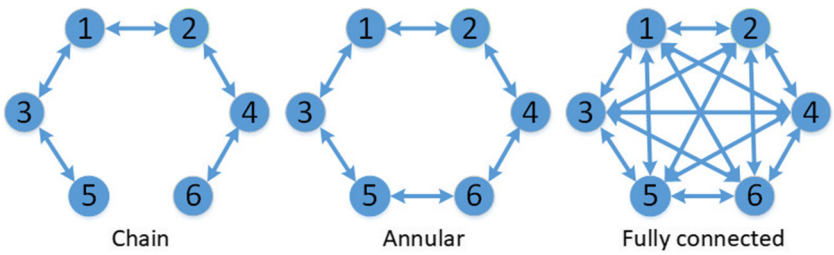

Fig. 4 The structures of biological CPG

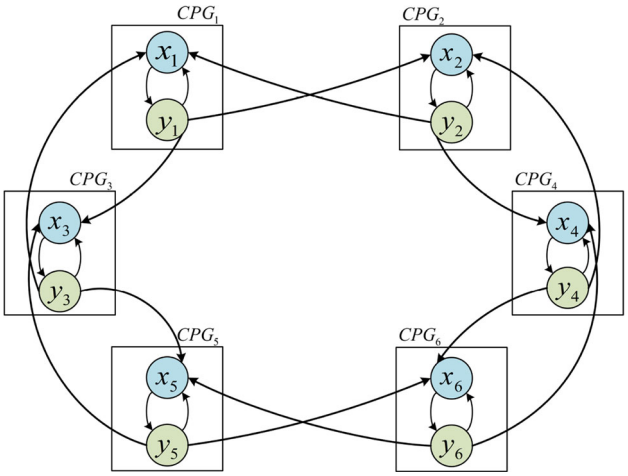

Fig. 5 CPG network topology of the system

where $X = [x_1, x_2, \cdots, x_6]^T$, $Y = [y_1, y_2, \cdots, y_6]^T$, $A = \text{diag}(\mu - x_1^2 - y_1^2, \cdots, \mu - x_6^2 - y_6^2)$, $W = \text{diag}(\omega_1, \cdots, \omega_6)$ and ε is the coupling strength between oscillators.

An antisymmetric coupling matrix $\boldsymbol{\theta} \in \mathbb{C}^{6\times 6}$ is defined to represent the phase relationships between oscillators. θ_{ij} represents the phase difference between oscillator CPG_i and CPG_j, $(i = 1, 2, \cdots, 6, j = 1, 2, \cdots, 6)$, where $\theta_{ij} = 0$ means same phase. The coupling coefficient matrices are defined as $\mathcal{M} = \cos\boldsymbol{\theta}$ and $\mathcal{N} = \sin\boldsymbol{\theta}$. $\theta_{ij} = *$ means that there is no connection between these two oscillators. In this case, we stipulate that the elements at corresponding position of $\mathcal{M}$ and $\mathcal{N}$ are 0.

According to the number of legs supported by robots, hexapod robot walking gait can be divided into three types, i.e., tripod gait, tetrapod gait and wave gait. Their characteristics are shown in Table 2. The legs in same group have the same phase, their phase difference is 0. The annular coupled networks with different gaits are shown in Fig. 6. Thus, the coupling matrices of three gaits are defined as follows

$$\boldsymbol{\theta}_{tri} = \begin{bmatrix} * & \pi & \pi & * & * & * \\ -\pi & * & * & -\pi & * & * \\ -\pi & * & * & * & -\pi & * \\ * & \pi & * & * & * & \pi \\ * & * & \pi & * & * & \pi \\ * & * & * & -\pi & -\pi & * \end{bmatrix}, \tag{6}$$

$$\boldsymbol{\theta}_{tetr} = \begin{bmatrix} * & 2/3\pi & 4/3\pi & * & * & * \\ -2/3\pi & * & * & -2/3\pi & * & * \\ -4/3\pi & * & * & * & -2/3\pi & * \\ * & 2/3\pi & * & * & * & 4/3\pi \\ * & * & 2/3\pi & * & * & 2/3\pi \\ * & * & * & -4/3\pi & -2/3\pi & * \end{bmatrix}, \tag{7}$$

$$\boldsymbol{\theta}_{wave} = \begin{bmatrix} * & \pi & 4/3\pi & * & * & * \\ -\pi & * & * & -2/3\pi & * & * \\ -4/3\pi & * & * & * & -2/3\pi & * \\ * & 2/3\pi & * & * & * & 4/3\pi \\ * & * & 2/3\pi & * & * & \pi \\ * & * & * & -4/3\pi & -\pi & * \end{bmatrix}. \tag{8}$$

3.2 Fuzzy Controller Design

As can be seen from the above analyses that gait planning based on CPG belongs to open-loop control. Without considering feedback, it is difficult to adapt to different environments to implement effective control for BLHR. At present, classical control methods include PID control, sliding mode control, fuzzy control and neural network control, etc. Among these, fuzzy control stands out as a mature intelligent control method that does not rely on accurate mathematical models of the controlled object. It operates on straightforward principles, is easily implementable, and demonstrates strong anti-interference capabilities. Thus, we propose a CPG-Fuzzy controller to implement heading control for BLHR.

In Fig. 3, ψ is the actual heading angle and ψ_d is the desired heading angle. k_e, k_{ec} and k_u are scale factors of inputs and outputs in fuzzy controller. $e(k)$ and $\Delta e(k)$ represent the heading error and the rate of error change, respectively.

$$\begin{cases} e(k) = \psi - \psi_d \\ \Delta e(k) = e(k) - e(k-1). \end{cases} \tag{9}$$

The inputs of the fuzzy controller are designed as $E = k_e e(k)$ and $EC = k_{ec}\Delta e(k)$. The outputs are u_i, $(i = 1, 2, \cdots, 6)$. We define $(\cdot)_l$ to represent the parameters of left legs, i.e., $i = 1, 3, 5$, while define $(\cdot)_r$ to represent the

Table 2 The Characteristic of Different Gaits

Gait	Group	Characteristic
Tripod gait	I:(1,4,5); II:(2,3,6)	One group legs are in the support phase simultaneously.
Tetrapod gait	I:(1,4); II:(2,5); III:(3,6)	Two groups legs are in support phase simultaneously.
Wave gait	I:(1); II:(4); III:(5); IV:(2); V:(3); VI:(6)	Five legs are in support phase simultaneously.

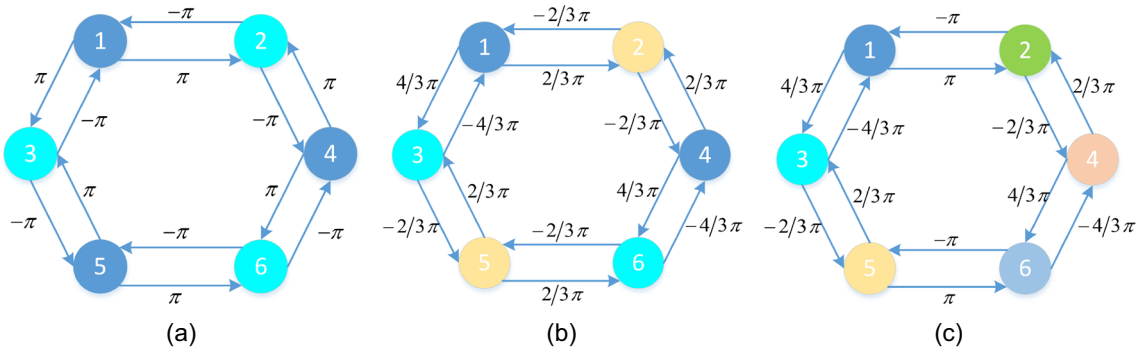

Fig. 6 The annular coupled networks with different gaits: (a) tripod gait; (b) tetrapod gait; (c) wave gait

parameters of right legs, i.e., $i = 2, 4, 6$. The basic universe of control inputs and outputs are $[-3, 3]$, and the basic universe is planned into 7 levels. The control inputs and outputs adopt the triangular membership function, and the fuzzy sets are all set as $\{NB, NM, NS, ZE, PS, PM, PB\}$, which correspond to Negative Big, Negative Middle, Negative Small, Zero, Positive Small, Positive Middle and Positive Big, respectively. The membership function is shown in Fig. 7.

The adjustment rule of u_i is: a) when $E > 0$, the BLHR is leaning to left and should turn right. θ_{sl} need increase and θ_{sr} need decrease, when EC is positive, u_l is positive and u_r is negative; b) when $E < 0$, the BLHR is leaning to right and should turn left. θ_{sl} need decrease and θ_{sr} need increase, when EC is negative, u_l is negative and u_r is positive. According to the adjustment rules of u_i, the fuzzy control rules of u_l and u_r are designed respectively, as shown in Tables 3 and 4.

Mamdani fuzzy reasoning method is used and the output vector of the fuzzy control quantity is obtained according to the maximum and minimum method. Defuzzification is the center of gravity method. The output surface of the model is shown in Fig. 8.

The actual change coefficients of the support angle is $k_i = k_u u_i$. The key point of the proposed controller is to adjust the heading by changing the support angle of the legs. The initial support angle is defined as θ_{s0}, and the real-time support angle of the legs is designed as

$$\theta_{si} = (1 + k_i)\theta_{s0}. \tag{10}$$

3.3 Mapping Function Between CPG Output and Joint Rotation Angle

After establishing the output waveform of the CPG network, the output signal is then translated into joint rotation angles. Each oscillator's state transition is depicted as a harmonic output signal, making it pivotal to create a mapping function between harmonic signals and the rhythmic movements of the robot in order to realize CPG bionic control.

We establish an one-to-one correspondence between the CPG output variable y_i and the joint rotation angle q_i. Since the variation range of y_i is $[-1, 1]$, the variation range of q_i is $[0, 2\pi]$, then, the mapping function can be designed as

$$q_i = \begin{cases} (1 + y_i) \times \theta_{s_i}/2 + \theta_{P_i}, & x_i \geq 0 \\ -(1 + y_i) \times \theta_{f_i}/2 + \theta_{P_i} + 2\pi, & x_i < 0. \end{cases} \tag{11}$$

Thus, the joint rotation angles of six legs are obtained, so as to adjust the heading of BLHR in real-time.

Remark 3 The BLHR integrates the strengths of both legged and wheeled robots, offering adaptability to diverse terrains. The proposed method proves effective in environments

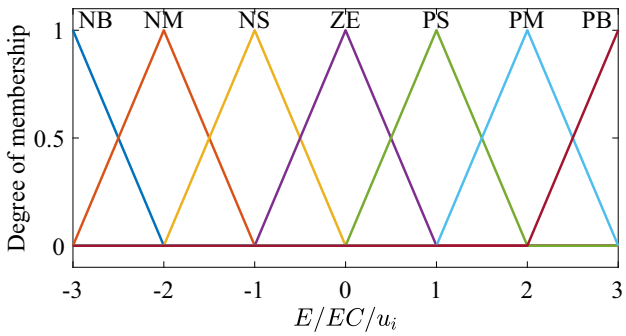

Fig. 7 The membership function of E, EC and u_i

Table 3 Fuzzy control rules of u_l

E \ EC	NB	NM	NS	ZE	PS	PM	PB
NB	NB	NB	NM	NM	NS	ZE	ZE
NM	NB	NB	NM	NS	NS	ZE	PS
NS	NM	NM	NS	NS	ZE	PS	PS
ZE	NM	NM	NS	ZE	PS	PM	PM
PS	NS	NS	ZE	PS	PS	PM	PM
PM	NS	ZE	PS	PS	PM	PB	PB
PB	ZE	ZE	PS	PM	PM	PB	PB

Table 4 Fuzzy control rules of u_r

E \ EC	NB	NM	NS	ZE	PS	PM	PB
NB	PB	PB	PM	PM	PS	ZE	ZE
NM	PB	PB	PM	PS	PS	ZE	NS
NS	PM	PM	PS	PS	ZE	NS	NS
ZE	PM	PM	PS	ZE	NS	NM	NM
PS	PS	PS	ZE	NS	NS	NM	NM
PM	PS	ZE	NS	NS	NM	NB	NB
PB	ZE	ZE	NS	NM	NM	NB	NB

requiring heading control. Nevertheless, it is noted that the proposed method may encounter limitations in terrains characterized by significant slopes, large obstacles, or extensive sand and gravel, where it might not be suitable for operation.

4 Simulation and Experiment

To validate the effectiveness of the proposed CPG-Fuzzy controller, we conducted two motion tests in both Gazebo simulations and real-world experiments. These tests encompass directional straight motion with three different gaits and directional turning motion with tripod gait.

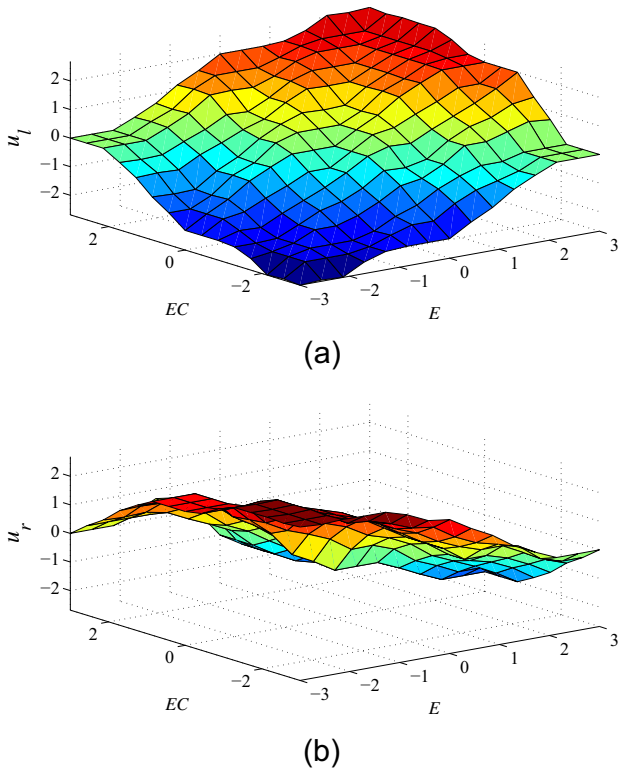

Fig. 8 The output surface of the fuzzy controller: (a) the output surface of u_l; (b) the output surface of u_r

4.1 Simulation

The principles of parameters selection are as follows. Firstly, the period T and duty cycle β are chosen, thereby determining the gait pattern to be employed. Subsequently, initial values of the coupled variables x and y are chosen. μ influences the amplitude of the oscillator's output, with a value range of $(0, +\infty)$. As μ increases, the oscillator's amplitude gradually grows. α affects the convergence rate of the limit cycle and with a value range of $(0, +\infty)$. As α increases, the convergence rate accelerates, but beyond a certain point, it no longer impacts the oscillator's output performance. b influences the waveform's period, with a larger b resulting in a longer period. However, beyond a certain value, it ceases to affects the oscillator's output performance. The values of k_e and k_{ec} impact the steady-state error and with a value range of $(0, +\infty)$. Larger parameter values lead to smaller errors. While k_u affects the magnitude of the support angle, with a value range of $[0, 1/3]$. Increasing k_u also increases the support angle.

Based on the above analysis, the parameters are selected as: $k_e = k_{ec} = 30$, $k_u = 1/3$, $\varepsilon = 0.001$, $\alpha = 2$, $\mu = 1$ and $\theta_{s0} = 0.52$. For tripod gait, $T = 1$, $\beta = 0.5$, $b = 10$, $x(0) = [0, 0, 0, 0, 0, 0]^{\mathrm{T}}$ and $y(0) = [1, -1, -1, 1, 1, -1]^{\mathrm{T}}$. For tetrapod gait, $T = 1$, $\beta = 0.667$, $b = 40$, $x(0) = [0, 1, 0, 0, 1, 0]^{\mathrm{T}}$ and $y(0) = [1, 0, -1, 1, 0, -1]^{\mathrm{T}}$. For wave gait, $T = 2$, $\beta = 0.833$, $b = 400$, $x(0) = [0, 0.95, 0.6, 0.6, 0.95, 0]^{\mathrm{T}}$ and $y(0) = [1, -0.3, -0.8, 0.8, 0.3, -1]^{\mathrm{T}}$.

Figures 9, 10 and 11 illustrate the CPG output and the joint rotation angle associated with different gaits. In the tripod gait, the sequence of leg movements is $(1, 4, 5) \rightarrow (2, 3, 6)$,

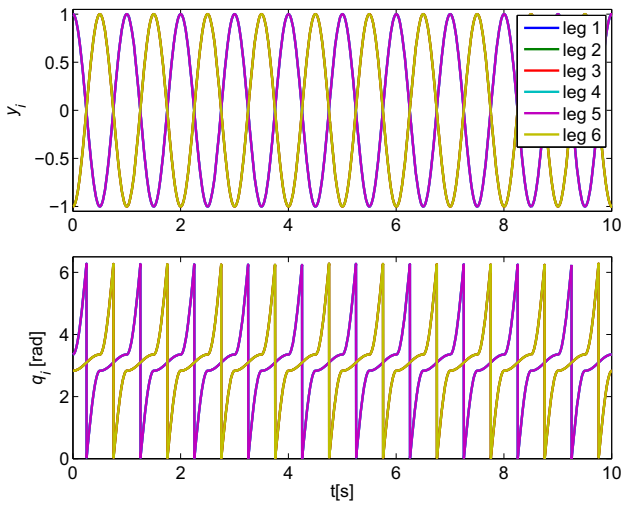

Fig. 9 CPG output y_i and the joint rotation angle q_i with tripod gait

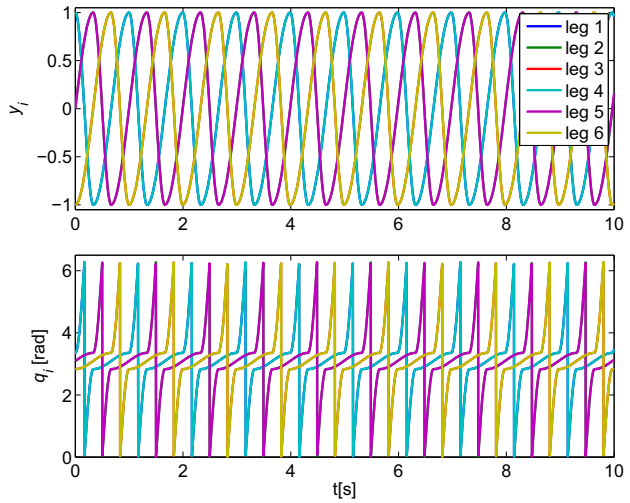

Fig. 10 CPG output y_i and the joint rotation angle q_i with tetrapod gait

while in the tetrapod gait, it is $(1, 4) \rightarrow (5, 2) \rightarrow (3, 6)$, and in the wave gait, it follows the sequence $1 \rightarrow 4 \rightarrow 5 \rightarrow 2 \rightarrow 3 \rightarrow 6$. These sequences correspond to the phase of the CPG output curve. Notably, the curves of the two groups of legs in tripod gait coincide with a phase difference of $T/2$. The curves of the three groups of legs in tetrapod gait coincide with a phase difference of $T/3$, while the phases of each leg in wave gait differ by $T/6$. These figures reveal that CPG can generate periodic curves, with the frequencies of the support and swing phases being adjusted independently.

Simulation 1: Directional straight motion Firstly, we subjected the proposed CPG-Fuzzy controller to a test for directional straight motion in Gazebo, setting both the initial and desired heading angles of BLHR to 0 rad. The heading angle curves of the CPG control method, CPG-Fuzzy control method, and the closed-loop CPG-based control method proposed in [9] are presented in Fig. 12. Notably, the CPG control method being open-loop, results in a continuous increase in heading angle. In contrast, both the CPG-Fuzzy method and the closed-loop CPG-based method successfully achieve directional straight motion. Within a 10 s span, the heading angle changes by 0.026 rad with tripod gait, 0.04 rad with tetrapod gait, and 0.08 rad with wave gait using the CPG-Fuzzy control method.

The comparisons of heading error between these three control methods are shown in Table 5. It is evident that the CPG-Fuzzy control method yields the smallest error. In comparison to conventional CPG method, the proposed method yields a substantial error reduction of 86% with tripod gait,

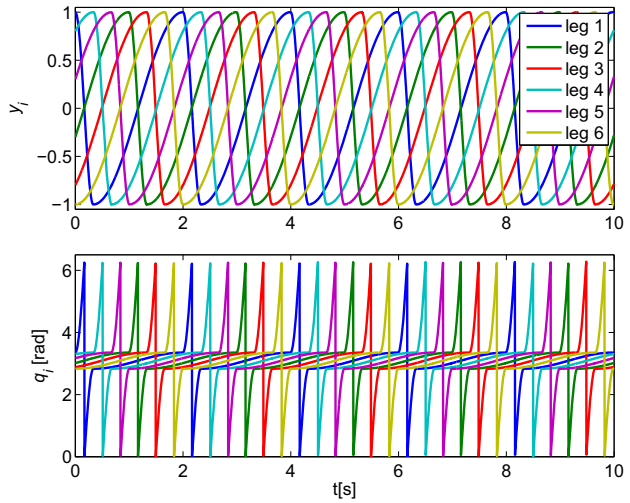

Fig. 11 CPG output y_i and the joint rotation angle q_i with wave gait

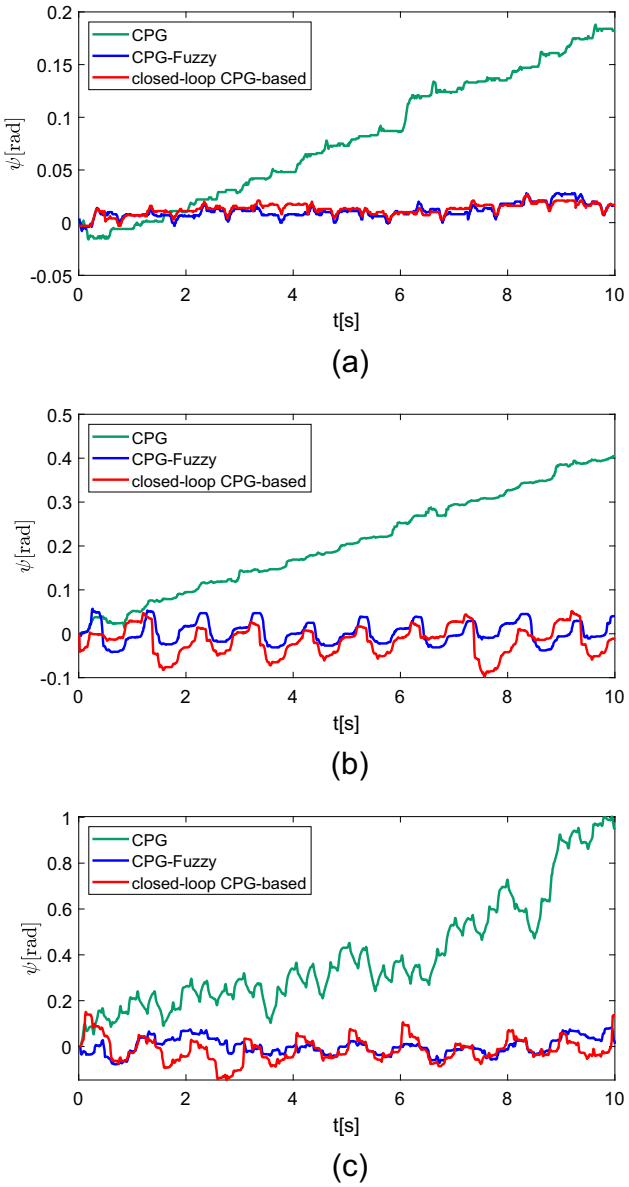

Fig. 12 Heading angle variation curve with different gait: (a) tripod gait; (b) tetrapod gait; (c) wave gait

Table 5 Comparison of heading error between three control methods

Method \ Gait	Tripod gait	Tetrapod gait	Wave gait
CPG	0.19 rad	0.41 rad	1 rad
CPG-Fuzzy	**0.026 rad**	**0.04 rad**	**0.08 rad**
closed-loop CPG-based	0.028 rad	0.1 rad	0.15 rad

90% with tetrapod gait, and 92% with wave gait. Notably, the error under each gait is even smaller than that observed in the closed-loop CPG method presented in [9]. This observation leads to the conclusion that the proposed CPG-Fuzzy controller enables better performance.

Simulation 2: Directional turning motion Subsequently, we configured the initial heading angle of BLHR to be 3.14 rad, with a desired heading angle of 2.74 rad, in order to evaluate the directional turning capability of the CPG-Fuzzy controller as proposed. The snapshots of BLHR's directional turning motion, executed with tripod gaits, within the Gazebo environment, are depicted in Fig. 13.

The rotation angle of each joint and its partial enlarged view are displayed in Fig. 14. Initially, there is a disparity between the heading angle of BLHR and the desired heading, resulting in large support angles for the right legs. Over time, these support angles progressively diminish until BLHR's heading aligns with the desired value. Subsequently, the support angles for both the left and right legs remain in close proximity, adjusting within a small range centered around θ_{s0}, ensuring that BLHR consistently maintains the desired heading angle.

The heading angle variation is depicted in Fig. 15. Employing the tripod gait, BLHR consistently fine-tunes its heading in response to the real-time heading angle, ultimately converging with the desired heading until 11.8 s. Subsequently, throughout the remainder of the operation, the heading angle remains steadfastly close to 2.74 rad, boasting a minimal heading tracking error of just 0.025 rad.

In Fig. 16, the support angles are illustrated. It's apparent that θ_{sr} decreases from 0.87 rad to 0.52 rad, while θ_{sl} increases from 0.17 rad to 0.52 rad, aligning with the fluctuations observed in q_i as shown in Fig. 14. Once BLHR

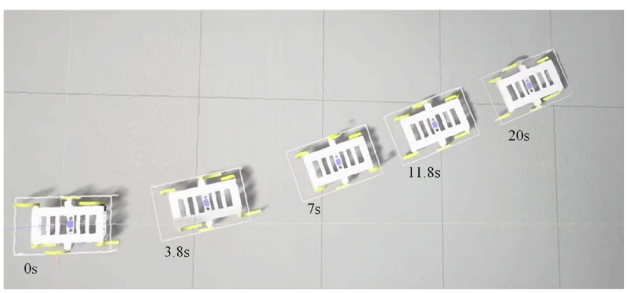

Fig. 13 The directional motion snapshots of BLHR with tripod gaits

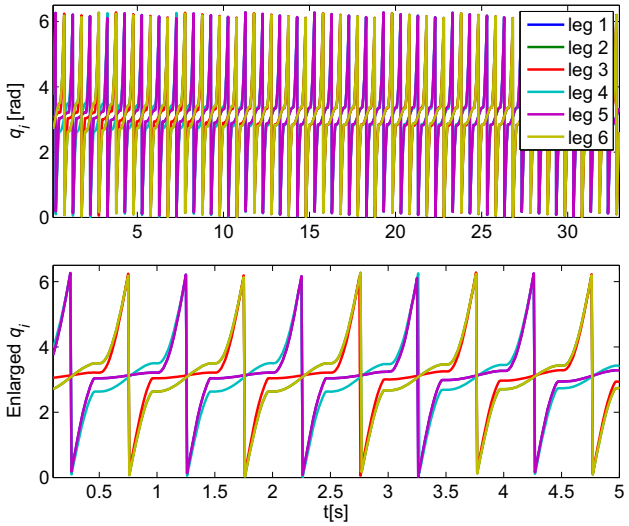

Fig. 14 The joint rotation angle of each leg

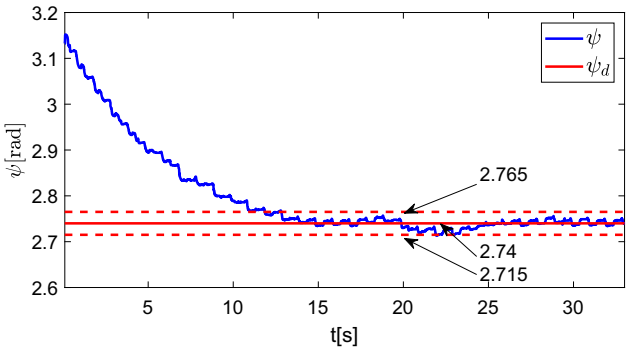

Fig. 15 The heading angle of directional control

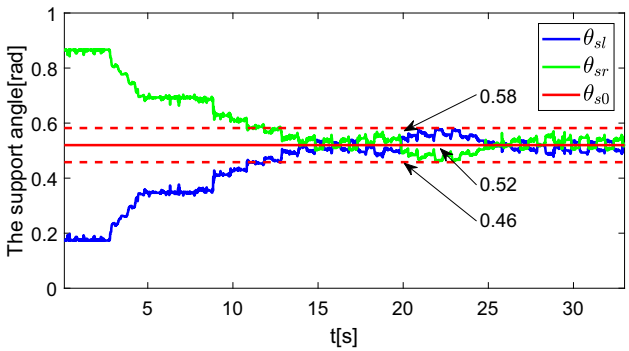

Fig. 16 The support angle θ_{si}

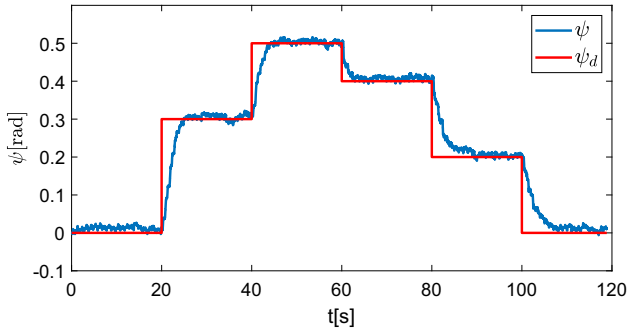

Fig. 17 The heading angle of continuous turning

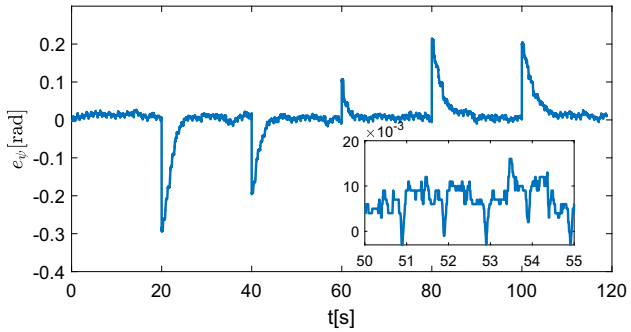

Fig. 18 The heading angle tracking error e_ψ

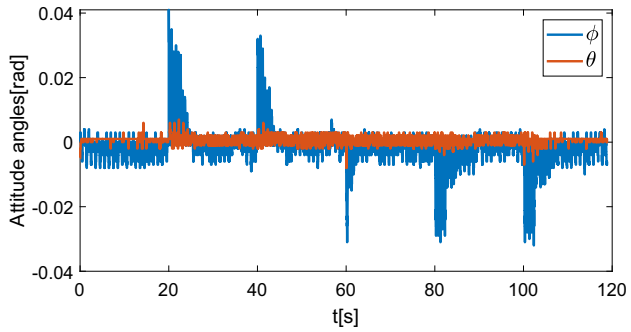

Fig. 19 The roll angle and pitch angle

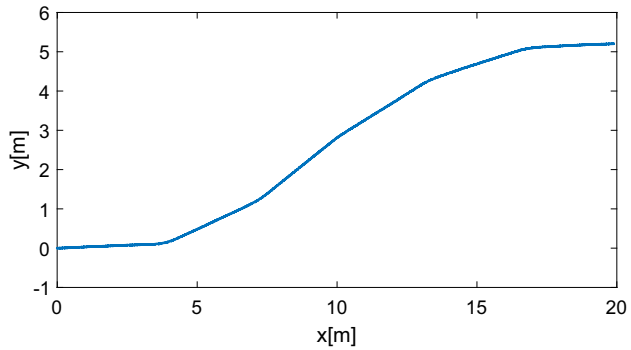

Fig. 20 The movement trajectory

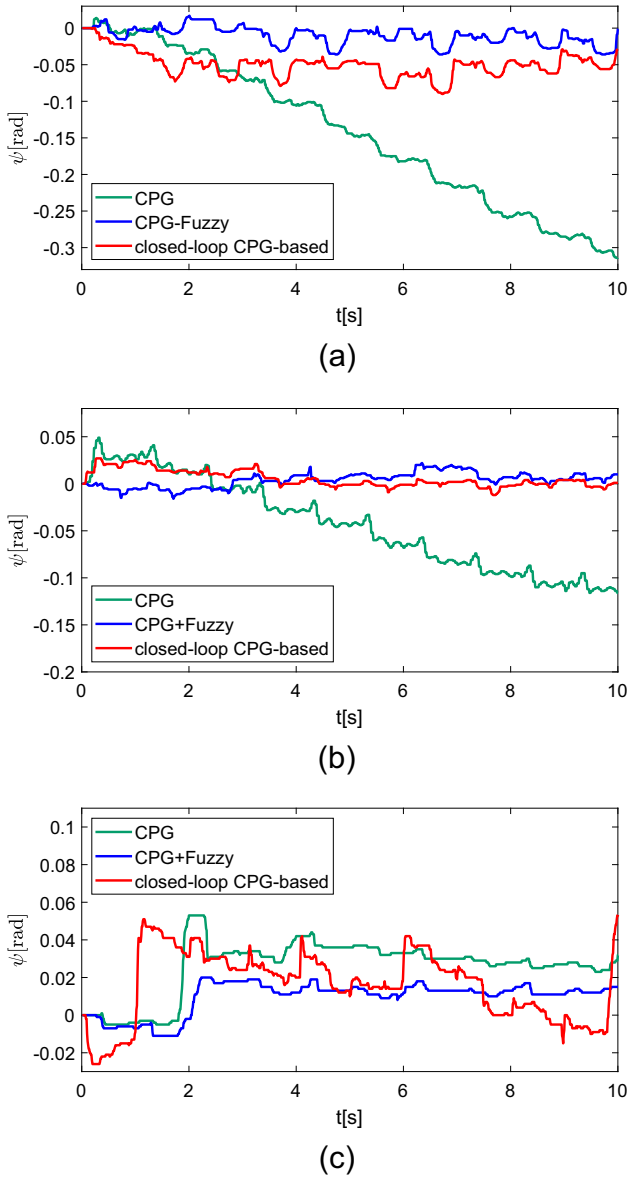

Fig. 21 Heading angle variation curve with different gait: (a) tripod gait; (b) tetrapod gait; (c) wave gait

achieves its desired heading, the support angles for the left and right legs stabilize at approximately 0.52 rad, with fine-tuning that maintains them within a constrained margin of 0.06 rad.

To further validate the effectiveness of the proposed method, we have tested the situation of continuous turning motion. We initialized BLHR with a heading angle of 0 rad and introduced a time-varying desired heading angle as

Table 6 Comparison of heading error between three control methods

Method \ Gait	Tripod gait	Tetrapod gait	Wave gait
CPG	0.32 rad	0.12 rad	0.052 rad
CPG-Fuzzy	**0.03 rad**	**0.02 rad**	**0.02 rad**
closed-loop CPG-based	0.09 rad	0.03 rad	0.051 rad

follows:

$$\psi_d = \begin{cases} 0, & 0 < t \leq 20 \\ 0.3, & 20 < t \leq 40 \\ 0.5, & 40 < t \leq 60 \\ 0.4, & 60 < t \leq 80 \\ 0.2, & 80 < t \leq 100 \\ 0, & t > 100. \end{cases}$$

The heading angle of continuous turning of BLHR is depicted in Fig. 17. Regardless of varying heading targets, BLHR consistently demonstrates rapid responsiveness, reaching the desired heading angle. The corresponding heading angle tracking error, denoted as $e_\psi = \psi - \psi_d$, is illustrated in Fig. 18. It is evident that BLHR consistently maintains its motion within an error margin of 0.02 rad after achieving the desired heading. Additionally, the data reveals that it takes approximately 4 s to reach the desired heading angle when $e_\psi = 0.3$ rad, 3.3 s when $e_\psi = 0.2$ rad, and 1.6 s when $e_\psi = 0.1$ rad.

The attitude angles are illustrated in Fig. 19. Analysis of the data reveals that the maximum roll angle is $\phi_{max} = 0.04$ rad, the average roll angle is $\phi_{ave} = 0.0016$ rad, the maximum pitch angle is $\theta_{max} = 0.007$ rad and the average pitch angle is $\theta_{ave} = 0.0006$ rad. Considering the dimensions of BLHR, the maximum longitudinal and lateral displacements amount to 16.97 mm and 4.06 mm, respectively. In relation to the BLHR's body proportions, these deviations are minuscule, resulting in negligible effects on the BLHR's stability. The movement trajectory is visualized in Fig. 20. From each curve segment in the trajectory, it is evident that the robot quickly reaches the desired heading and maintains a fixed heading motion. Thus, the BLHR achieves continuous turning motion.

4.2 Experiments

Subsequently, we assess the effectiveness of the proposed method for BLHR by conducting experiments in an indoor hallway.

Experiment 1: Directional straight motion To evaluate the performance of the proposed CPG-Fuzzy controller for directional straight motion, both the initial and desired heading angles of BLHR were set to 0 rad. The variation curves in heading angle with various gaits are represented in Fig. 21. Comparisons of heading errors among the CPG control method, CPG-Fuzzy control method, and the closed-loop CPG-based control method presented in [9] can be found in Table 6. The heading error trends for these different control methods closely mimic those observed in the simulations. The proposed method yields a substantial error reduction of 91% with tripod gait, 83% with tetrapod gait, and 62% with wave gait compared with conventional CPG method. It is evident that the proposed CPG-Fuzzy controller delivers better performance.

Experiment 2: Directional turning motion Similarly, we introduced a 0.4 rad variation by setting the initial heading angle of BLHR to 1 rad and the desired heading angle to 1.4 rad, assessing the directional turning functionality of the proposed CPG-Fuzzy controller.

The variation curve of the heading angle is depicted in Fig. 22. Employing the tripod gait, BLHR consistently adapts its heading, reaching the desired angle within 4.9 seconds.

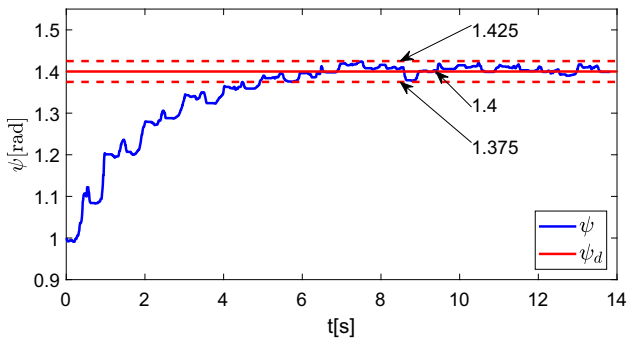

Fig. 22 The heading angle of directional control

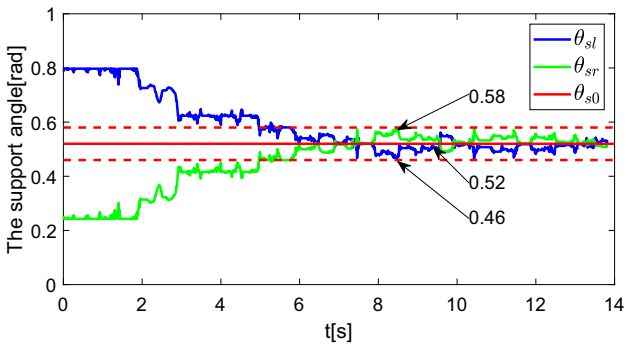

Fig. 23 The support angle θ_{si}

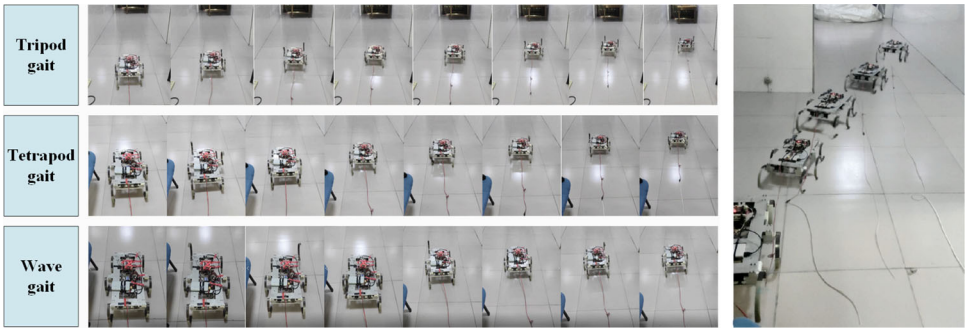

Fig. 24 Walking movement snapshots of BLHR. (a) Direction straight motion with different gaits; (b) Direction turning motion with tripod gait (Video link: https://www.youtube.com/watch?v=5kM-E-TzCbA)

Subsequently, throughout the remainder of the operation, the heading angle remains consistently close to 1.4 rad, exhibiting a minor heading tracking error of just 0.025 rad. This signifies the successful achievement of heading control for BLHR. Figure 23 displays the support angles. Notably, θ_{sr} exhibits an increase from 0.24 rad to 0.52 rad, while θ_{sl} experiences a decrease from 0.8 rad to 0.52 rad. This aligns with the same change trend observed in the simulation for θ_{si}. The walking movement snapshots of BLHR in real-world are depicted in Fig. 24.

5 Conclusion

In this paper, a heading control method for the directional motion of the hexapod robot driven by arc-shaped blade legs is proposed, employing the combination of CPG and fuzzy controller. The CPG model of BLHR is constructed using the modified Hopf oscillator and the CPG structure is designed as an annular coupling network. The adjustment coefficient of the support phase angle of legs is determined using fuzzy controller according to heading error, so as to adjustment the heading of BLHR in real-time. Through the heading motion of BLHR using CPG-Fuzzy controller, the errors of the three different gaits are smaller than the CPG control method and closed-loop CPG-based control method in Gazebo and real-world environments, which verifies the feasibility and effectiveness of the proposed method. Future research efforts will delve into path tracking control that simultaneously considers speed and heading, building upon the findings presented in this paper. Additionally, there will be an investigation into validating the effectiveness of the controller under more complex and challenging working conditions.

Acknowledgements This work was supported by the National Natural Science Foundation of China under Grant (No. U22A2066, U21B2047 and 62103182); and the Fundamental Research Funds for the Central Universities under Grant (No.G2023KY05104).

Author Contributions Yani Zhang: Conceptualization, Methodology, Writing-original draft. Rongxin Cui: Supervision, Writing-review and editing. Haoquan Li: Methodology. Xinxin Guo: Supervision, Writing-review and editing.

Code or Data Availability Not applicable.

Declarations

Competing interests The authors have no relevant financial or non-financial interests to disclose.

Ethics Approval Not applicable.

Consent to Participate Not applicable.

Consent for Publication Not applicable.

References

1. Rudin, N., Kolvenbach, H., Tsounis, V., Hutter, M.: Cat-like jumping and landing of legged robots in low-gravity using deep reinforcement learning. IEEE Trans. Robot. **38**(1), 317–328 (2021)
2. Kameduła, M., Tsagarakis, N.G.: Reactive support polygon adaptation for the hybrid legged-wheeled centauro robot. IEEE Robot Autom Lett. **5**(2), 1734–1741 (2020)
3. Orozco-Magdaleno, E.C., Cafolla, D., Castillo-Castaneda, E., Carbone, G.: Static balancing of wheeled-legged hexapod robots. Robotics **9**(2), 23–35 (2020)
4. Zhang, G., Ma, S., Liu, J., Zeng, X., Kong, L., Li, Y.: Q-whex: A simple and highly mobile quasi-wheeled hexapod robot. J Field Robot. 1–16 (2023)

5. Xu, Y., Gao, F., Pan, Y., Chai, X.: Hexapod adaptive gait inspired by human behavior for six-legged robot without force sensor. J. Intell. Robot. Syst. **88**, 19–35 (2017)
6. Yang, W., Lu, W., Lin, P.: Legged robot running using a physics-data hybrid motion template. IEEE Trans. Robot. **37**(5), 1680–1695 (2021)
7. Saranli, U., Buehler, M., Koditschek, D.E.: Rhex: A simple and highly mobile hexapod robot. Int J Rob Res. **20**(7), 616–631 (2001)
8. Schroer, R.T., Boggess, M.J., Bachmann, R.J., Quinn, R.D., Ritzmann, R.E.: Comparing cockroach and whegs robot body motions. In: IEEE Int Conf Robot Autom., **4**, 3288–3293 (2004)
9. Ma, F., Yan, W., Chen, L., Cui, R.: Cpg-based motion planning of hybrid underwater hexapod robot for wall climbing and transition. IEEE Robot Autom Lett. **7**(4), 12299–12306 (2022)
10. Zhong, B., Zhang, S., Xu, M., Zhou, Y., Fang, T., Li, W.: On a cpg-based hexapod robot: Amphihex-ii with variable stiffness legs. IEEE ASME Trans Mechatron. **23**(2), 542–551 (2018)
11. Zhong, G., Chen, L., Jiao, Z., Li, J., Deng, H.: Locomotion control and gait planning of a novel hexapod robot using biomimetic neurons. IEEE Trans. Control Syst. Technol. **26**(2), 624–636 (2017)
12. Chen, Z., Li, J., Wang, S., Wang, J., Ma, L.: Flexible gait transition for six wheel-legged robot with unstructured terrains. Rob Auton Syst. **150**, 103989–104007 (2022)
13. Chang, Q., Mei, F.: A bioinspired gait transition model for a hexapod robot. J Robot. **2018**, 1–11 (2018)
14. Bellegarda, G., Ijspeert, A.: Cpg-rl: Learning central pattern generators for quadruped locomotion. IEEE Robot Autom Lett. **7**(4), 12547–12554 (2022)
15. Cristianoa, J., García, M.A., Puig, D.: Deterministic phase resetting with predefined response time for cpg networks based on matsuoka's oscillator. Rob Auton Syst. **74**, 88–96 (2015)
16. Kimura, H., Fukuoka, Y., Cohen, A.H.: Adaptive dynamic walking of a quadruped robot on natural ground based on biological concepts. Int J Rob Res. **26**(5), 475–490 (2007)
17. Ijspeert, A.J., Crespi, A., Ryczko, D., Cabelguen, J.M.: From swimming to walking with a salamander robot driven by a spinal cord model. Science **315**(04), 1416–1420 (2007)
18. Yu, H., Gao, H., Ding, L., Li, M., Deng, Z., Liu, G.: Gait generation with smooth transition using cpg-based locomotion control for hexapod walking robot. IEEE Trans. Ind. Electron. **63**(9), 5488–5500 (2016)
19. Felix, R., Alexander, B.S.: Learning plastic matching of robot dynamics in closed-loop central pattern generators. Nat Mach Intell. **7**(4), 652–660 (2022)
20. Righetti, L., Ijspeert, A.J.: Pattern generators with sensory feedback for the control of quadruped locomotion. In: IEEE Int Conf Robot Autom. (2008)
21. Santos, C.P., Matos, V.: Gait transition and modulation in a quadruped robot: A brainstem-like modulation approach. Rob Auton Syst. **59**(9), 620–634 (2011)
22. Lindqvist, B., Karlsson, S., Koval, A., Tevetzidis, I., Haluška, J., Kanellakis, C., Agha-mohammadi, A.a., Nikolakopoulos, G.: Multimodality robotic systems: Integrated combined legged-aerial mobility for subterranean search-and-rescue. Rob Auton Syst. **154**, 104134–104149 (2022)
23. Li, J., Wu, Q., Wang, J., Li, J.: Neural networks-based sliding mode tracking control for the four wheel-legged robot under uncertain interaction. Int J Robust Nonlin **31**(9), 4306–4323 (2021)
24. Yu, J., Wu, Z., Wang, M., Tan, M.: Cpg network optimization for a biomimetic robotic fish via pso. IEEE Trans Neural Netw Learn Syst. **27**(9), 1962–1968 (2016)
25. Korkmaz, D., Ozmen Koca, G., Li, G., Bal, C., Ay, M., Akpolat, Z.H.: Locomotion control of a biomimetic robotic fish based on closed loop sensory feedback cpg model. J Mar Eng Technol. **20**(2), 125–137 (2021)
26. Yan, Z., Yang, H., Zhang, W., Gong, Q., Lin, F., Zhang, Y.: Bionic fish trajectory tracking based on a cpg and model predictive control. J. Intell. Robot. Syst. **105**(2), 29–46 (2022)
27. Nguyen, V., Vo, D.Q., Duong, V., Nguyen, H.H., Nguyen, T.T.: Reinforcement learning-based optimization of locomotion controller using multiple coupled cpg oscillators for elongated undulating fin propulsion. Math. Biosci. Eng. **19**(1), 738–758 (2021)

Yani Zhang received the B.Eng. degree in Automatic Control from Xi'an University of Technology, Xi'an, China, in 2016, the M.S. degree in Armament Science and Technology from Northwestern Polytechnical University, Xi'an, China, in 2019. She is currently pursuing the Ph.D. degree in Armament Science and Technology with the School of Marine Science and Technology, Northwestern Polytechnical University, Xi'an, China. Her research interests include gait planning, robot locomotion and adaptive control.

Rongxin Cui received the B.Eng. degree in Automatic Control and Ph.D. degrees in Control Science and Engineering from Northwestern Polytechnical University, Xi'an, China, in 2003 and 2008, respectively. From August 2008 to August 2010, he was a Research Fellow at the Centre for Offshore Research & Engineering, National University of Singapore, Singapore. Currently, he is a Professor with the School of Marine Science and Technology, Northwestern Polytechnical University, Xi'an, China. His current research interests include control of nonlinear systems, cooperative path planning and control for multiple robots, control and navigation for underwater vehicles, and system development.

Haoquan Li received the B.Eng. degree in Mechanical Design, Manufacturing and Automation from Northwestern Polytechnical University, Xi'an, China, in 2017, and the M.S. degree in Armament Science and Technology from Northwestern Polytechnical University, Xi'an, China, in 2020. He is currently pursuing the Ph.D. degree in Armament Science and Technology with the School of Marine Science and Technology, Northwestern Polytechnical University, Xi'an, China. His research interests include robot system design and motion control.

Xinxin Guo received the B.Eng. degree in Automatic Control from Dalian University of Technology, Dalian, China, in 2011, M.S. degree in Control Theory and Engineering from Yichang Testing Technology Institute, Yichang, China, in 2014, and Ph.D. degree in Control Science and Engineering from Northwestern Polytechnical University, Xi'an, China, in 2020. From 2020 to 2022, she was a Postdoctoral Fellow at the Department of Mechanical and Energy Engineering, Southern University of Science and Technology, Shenzhen, China. She is currently an Associate Professor with the School of Marine Science and Technology, Northwestern Polytechnical University, Xi'an, China. Her research interests include differential games, adaptive control and reinforcement learning.